Optimal Single-Walled Carbon Nanotube Vessels for Short-Term Reversible Storage of Carbon Dioxide at Ambient Temperatures

Piotr Kowalczyk,*,†,§ Sylwester Furmaniak,‡ Piotr A. Gauden,‡ and Artur P. Terzyk‡

Nanochemistry Research Institute, Department of Chemistry, Curtin University of Technology, P.O. Box U1987, Perth, 6845 Western Australia, Australia, Applied Physics, RMIT University, GPO Box 2476 V, Victoria 3001, Australia, and Physicochemistry of Carbon Materials Research Group, Department of Chemistry, N. Copernicus University, Gagarin Street 7, 87-100 Torun, Poland

Received: July 14, 2010; Revised Manuscript Received: September 24, 2010

Optimized light vessels composed of single-walled carbon nanotubes have high gravimetric and volumetric capacity for short-term reversible storage of CO_2 at 298 K and near-ambient operating pressures. We use grand canonical Monte Carlo simulation for modeling of CO_2 adsorption at 298 K and pressures up to 5.7 MPa. It is shown that both gravimetric and volumetric uptake of CO_2 strongly depend on the pore size in nanotubes but not on their chiral vector. Moreover, for any operating storage pressure, a unique optimal size of carbon nanotubes is well-defined. At 1.5 MPa, the most efficient nanotubes that maximize both gravimetric and volumetric uptake of CO_2 (i.e., 13.6 mmol g^{-1} and 11.4 mol dm^{-3}) have diameters of 3.8 nm. This size corresponds to the (28,28) armchair nanotubes. For a higher operating pressure of 3.5 MPa, the optimal diameter of carbon nanotubes is slightly shifted up to 4.8 nm (i.e., 25.3 mmol g^{-1} and 16.7 mol dm^{-3}). This size corresponds to the (36,36) armchair nanotubes. We demonstrate that to make an objective statement about the efficiency of CO_2 storage in any nanoporous material, the complete volumetric and gravimetric adsorption data are necessary. Taking this into account, we discuss the recently reported exceptionally high capacity of metal−organic frameworks. We show that MOF-177, known as the most efficient porous material for storage of CO_2 at room temperature, is characterized by very high gravimetric uptake of CO_2 (i.e., 21.8 mmol g^{-1} at 1.5 MPa and 33.5 mmol g^{-1} at 3.5 MPa). However, the reported volumetric density of CO_2 adsorbed in MOF-177 at 298 K (i.e., 8.17 mol dm^{-3} at 1.5 MPa and 12.26 mol dm^{-3} at 3.5 MPa) is lower in comparison to storage vessels composed of optimized single-walled carbon nanotubes. Our systematic study of CO_2 adsorption in bundles composed of singe-walled carbon nanotubes at 298 K indicates the potential of nanotubes for innovation in clean technologies.

1. Introduction

Uncontrollable release of large quantities of CO_2 into the atmosphere has devastating environmental effects that include melting the polar ice caps and changing the ocean's acidity.[1−10] Thus, development of new as well as improvements of existing CO_2 capture technologies (i.e., flue gas purification, CO_2 geosequestration, fixation of CO_2 in photosynthesis, ocean CO_2 sequestration, chemical fixation of CO_2, etc.)[11−26] is an important and complex economic challenge. CO_2 adsorption and separation using a variety of porous materials has received much attention in the last decades. The most common ordinary porous adsorbents that have been widely used in industrial separations and storage of different fluid mixtures are activated carbons and zeolites.[27−34] Recently, new classes of storage vessels and membranes that can store and separate vast amounts of fluids has been discovered. Among them, crystalline metal−organic frameworks (MOFs)[14,15,35−42] and ordered carbonaceous materials [such as single-walled carbon nanotubes (SWNTs), multiwalled carbon nanotubes (MWNTs), wormlike nanotubes, double-walled carbon nanotubes, single-walled carbon nanohorns, stacked-cup carbon nanofibers, doped fullerenes, wormlike graphitic carbon nanofibers, bamboo-type multiwalled carbon nanotubes, activated carbon fibres, ordered porous carbons, etc.][43−56] are of great potential for reduction of CO_2 emissions near ambient temperatures by capture and short-term reversible storage. However, fundamental understanding of the competition between the space available for guest molecules and the high binding energy of adsorption at the nanoscale is crucial for designing of efficient nonporous membranes as well as storage vessels. Computer simulations supplemented with fundamental theory of physical adsorption offer an alternative tool for the systematic investigation of CO_2 adsorption and separation in different known and theoretical nanostructures. When the underlying physical conditions and the intermolecular potentials are known, computer simulations are convenient tools for extrapolating experimental results to conditions difficult to access experimentally (i.e., well-defined samples of nanomaterials, high purity of nanomaterials, broad spectrum of pore sizes, different operating conditions, unlimited access to different quantities characterized by the adsorption process, observation of adsorption phenomena at the molecular level, etc.).[57,58]

As was shown by Cinke et al.,[59] the adsorption characteristics of raw SWNTs are strongly influenced by those of Fe_2O_3. The metal and metal oxide impurities drastically lower the CO_2 uptake in SWNTs due to the weak CO_2−Fe_2O_3 binding energy (i.e., type III of the CO_2 adsorption isotherm on Fe_2O_3 according to IUPAC classification[60]) and high molecular weight of metal/

* To whom correspondence should be addressed. Tel: +61 (03) 99252571. Fax: +61 (03) 99255290. E-mail: piotr.kowalczyk@rmit.edu.au.
† RMIT University.
‡ N. Copernicus University.
§ Curtin University of Technology.

10.1021/jp106547j
Published on Web 11/12/2010

metal oxides in comparison to that of pure carbon. Purification of SWNTs results in almost twice larger adsorbed volumetric uptake of CO_2 compared to that of activated carbon (Calgon Corporation). This experimental result is particularly interesting since both studied carbonaceous materials are characterized by a similar order of apparent surface area computed from the Brunauer−Emmett−Teller method[61] (1617 and 1284 $m^2\ g^{-1}$ for purified SWNTs and activated carbon, respectively). The enthalpy of CO_2 adsorption in purified SWNTs of 23.03 kJ mol^{-1} results from strong physisorption of CO_2 at 308 K. High uptake of CO_2 of ∼4 mol dm^{-3} at 0.13 MPa and 308 K reveals the potential of purified SWNTs for greenhouse gas detection and bioremediation. Shen and Bai[62] synthetised open-ended MWNTs doped with various contents of nitrogen. These novel MWNTs possess high CO_2/CH_4 adsorption selectivity of 6−13 at zero coverage, which increases with increasing nitrogen content. Large apparent BET surface areas (400−500 $m^2\ g^{-1}$), uniform pore size distributions, and various contents of doped nitrogen impact the binding energy of mixture components (CO_2 and CH_4) with MWNT samples. However, one should remember that smart tuning of CO_2/CH_4 selectivity in any carbon nanotubes requires atomistic-level understanding of complex processes accompanying mixture adsorption. The experimental results of Hsu et al.[63] showed that SWNTs as well as MWNTs can be used as cost-effective sorbents for CO_2 capture from flue gas. As reported, adsorption capacities and physiochemical properties of studied carbon nanotubes were preserved during 20 cycles of adsorption and regeneration. Adsorption and selective properties of these carbon nanotubes were enhanced by functionalization with amines. As pointed out by the authors, amine-modified carbon nanotubes adsorbed twice the amount compared to that of amine-doped granular activated carbon. This experimental finding seems to be very interesting because both commercialized amine-doped granular activated carbons and novel amine-doped carbon nanotubes are characterized by a similar enthalpy of CO_2 adsorption (∼20.3 and 14−24 kJ mol^{-1} for activated carbons and amide-modified carbon nanotubes, respectively). Huang et al.[64] used grand canonical Monte Carlo (GCMC) simulations to investigate adsorption behavior of an equimolar CO_2/CH_4 mixture in carbon nanotubes. According to this study, isolated SWNTs demonstrated higher selectivity of CO_2 than other materials (activated carbons, zeolite 13X, and MOFs) reported in the literature. Huang et al.[64] showed that despite the change in temperature or pressure or for different carbon nanotube diameters, the selectivity is generally above 8. At 343 K and 1 MPa, the selectivity reaches 11.2 in the (6,6) carbon nanotube, which is larger than ever reported in activated carbon (selectivity of 4) and MOFs (selectivity of 10). This theoretical study showed the potential of SWNTs for separation of CO_2/CH_4 mixtures under assumed thermodynamic equilibrium. However, one should keep in mind that the model of the isolated carbon nanotube does not corresponds to real assembly of SWNTs. Due to action of attractive van der Waals forces between carbon atoms, individual carbon nanotubes self-assemble into a stable bundle structure.[65−68] The overall selectivity of this entanglement structure depends on the selectivity of different adsorption sites, including internal and interstitial channels, grooves, and the rounded surface of the bundle. Isolation and separation of individual carbon nanotubes are difficult and expensive processes. That is why the model of the isolated carbon nanotube is a crude approximation to the real carbon nanomaterials composed of self-assembled carbon nanotubes. Chen and Johnson[69] showed that CO_2 adsorbed in the groove sites of SWNTs displays unique quasi-one-dimensional behavior. Interestingly, they showed that clusters containing only odd numbers of molecules are formed at finite CO_2 coverages and low temperatures. Following Chen and Johnson,[69] this ordering is a result of a delicate balance between solid−fluid and fluid−fluid forces. Moreover, as shown by the authors, the CO_2 quadrupole plays a critical role in the cluster formation and orientational ordering. Concluding, previous simulations indicated that any realistic modeling of CO_2 adsorption and separation in carbonaceous nanomaterials composed of carbon nanotubes should employ a fully atomistic model of CO_2.

The above-quoted experimental and theoretical results indicate that various pure and modified carbon nanotubes are promising for innovations in CO_2 short-term reversible storage, separation, and sensing technologies. The transportation of CO_2 from the power plant to the place of its geosequestration exceeds 90% of the overall cost. Thus, reversible short-term storage of CO_2 in nanoporous materials is an interesting alternative for high-energy consumption processes accompanying CO_2 transportation, such as compression or liquefaction. Experimental results clearly show that various pure and modified carbon nanotubes adsorbed more CO_2 in comparison to commercial granular activated carbons, regardless of similar apparent surface area or enthalpy of adsorption. Nevertheless, no general conclusions or clear future directions connected with the optimal size of carbon nanotubes for short-term reversible storage of CO_2 near ambient conditions have been presented. That is why the atomistic-level understanding of the CO_2 adsorption mechanism in realistic SWNTs bundles seems to be very important for optimization of potential CO_2 storage vessels, molecular sieves, and sensors. In the current work, we want to find answers to the following questions: (1) What is the optimal size of carbon nanotubes for short-term reversible storage of pure CO_2 at 298 K? (2) Does an optimal size of carbon nanotubes for adsorption of pure CO_2 depend on the operating storage pressure? (3) What is the magnitude of volumetric and gravimetric uptake of CO_2 in optimized SWNT bundles? (4) What is the potential of carbon nanotubes for CO_2 capture in comparison to selected MOFs, zeolites, and activated carbons? To answer these questions, we performed extensive computer simulations of CO_2 adsorption at 298 K and pressures up to 5.7 MPa in realistic bundles composed of different SWNTs. In the section 2, we briefly present simulation details including intermolecular potentials, simulation details, and macroscopic quantities characterized by the adsorption process. Next, we present our theoretical results in close relation to known experimental data. Here, we compare and discuss the CO_2 adsorption properties of studied SWNT bundles and other novel and ordinary porous materials. Finally, we present conclusions. Our simulation results can be interesting for postcombustion CO_2 capture and short-term reversible storage.

2. Simulation Methodology

2.1. Interaction Potentials. Carbon dioxide was modeled by a three-center rigid model (with a fixed C−O bond length of 0.1162 nm).[13,70] Each center was the (12,6) Lennard-Jones one (LJ) as well as the point charge (Q). The total energy of interactions between a pair of CO_2 molecules A and B can be written as[13,70]

$$U_{FF}^{(A,B)} = \sum_{i=1}^{3}\sum_{j=1}^{3}[U_{LJ}^{(A,B)}(r_{ij}) + U_{Q}^{(A,B)}(r_{ij})] \qquad (1)$$

TABLE 1: Values of the (12,6) LJ Parameters and the Point Charges Used in the Current Study of CO_2 Adsorption in Carbon Nanomaterials Composed of Single-Walled Nanotubes

molecule/structure	center	σ_{ii}, [nm]	ε_{ii}/k_B, [K]	q/e	reference
CO_2	C	0.2824	28.68	0.664	78
	O	0.3026	82.00	−0.332	
nanotubes	C	0.3400	28.0		70

where $U_{LJ}^{(A,B)}(r_{ij})$ is the energy of dispersion interactions between center i on molecule A and center j on molecule B. The dispersion interactions were computed from the truncated (12,6) LJ potential[71,72]

$$U_{LJ}^{(A,B)}(r_{ij}) = \begin{cases} 4\varepsilon_{ij}\left[\left(\frac{\sigma_{ij}}{r_{ij}}\right)^{12} - \left(\frac{\sigma_{ij}}{r_{ij}}\right)^{6}\right] & r_{ij} < r_{CUT,LJ} \\ 0 & r_{ij} \geq r_{CUT,LJ} \end{cases} \quad (2)$$

where $\sigma_{ij}$and ε_{ij} are the collision diameter and depth of the potential well (see Table 1), and $r_{CUT,LJ}$ denotes the cutoff distance for dispersion interactions.

The second term in eq 1 is the energy of electrostatic interactions between point charge i on molecule A and point charge j on molecule B. We calculated electrostatic interactions from Coulomb's law[71,72]

$$U_{Q}^{(A,B)}(r_{ij}) = \begin{cases} \frac{1}{4\pi\varepsilon_0}\frac{q_i q_j}{r_{ij}} & r_{CC}^{(A,B)} < r_{CUT,Q} \\ 0 & r_{CC}^{(A,B)} \geq r_{CUT,Q} \end{cases} \quad (3)$$

where $r_{CC}^{(A,B)}$ is the distance between the centers of mass of the molecules A and B, q_i and q_j denote the values of the point charges, and ε_0 (8.8543×10^{-12} C^2 J^{-1} m^{-1}) is the permittivity of the free space. We use the cutoffs for electrostatic interactions, but for all molecules, if the centers of the mass of two molecules are located at a distance smaller than the cutoff for electrostatic interactions ($r_{CUT,Q}$, assumed to be equal to 1.5 nm), the sum of the energy of interactions between all pairs of charges occurring in the molecules is calculated; otherwise, the electrostatic interactions are neglected.[13,70] At this cutoff distance, the energy of interactions of a pair of molecules is negligibly small because the energy of electrostatic interactions for CO_2 molecules (having quadrupole moments) decreases proportionally to the fifth power of the distance.[73]

Total solid−fluid interactions between CO_2 molecule A and carbon nanomaterial include only dispersion interactions[13,70]

$$U_{SF}^{(A)} = \sum_{i=1}^{N_C}\sum_{j=1}^{3} U_{LJ}^{(A)}(r_{ij}) \quad (4)$$

where N_C denotes the number of carbon atoms in the simulation box. For all (12,6) LJ interactions, the cutoffs were placed at $r_{CUT,LJ} = 5\sigma_{ij}$.[13,70] All parameters used in computer simulations are displayed in Table 1. As previously, we used Lorentz−Berthelot mixing rules for all cross-term interactions.[71,72] Aldought application of the Lorentz−Berthelot mixing rule for calculation of cross-term interactions is justified for mixtures of nobles gases, our previous simulation results indicate that this mixing rule correctly reproduces the fundamental adsorption properties of fluids in various nanoporous materials. To justify used solid−fluid LJ parameters, we compared CO_2 adsorption properties computed for selected values of the LJ well depth. Increasing of the solid−fluid LJ well depth predicted from the Lorentz−Berthelot mixing rule by 5% has negligible impact on the computed absolute value and enthalpy of CO_2 adsorption in optimized carbon nanomaterials (see Figure 1S and 2S in the Supporting Information).

2.2. Simulation Details. We simulated CO_2 adsorption isotherms by the GCMC method.[71,72] We adopted our previous setup for GCMC simulation of adsorption in bundles composed of SWNTs, that is, a cubicoid simulation box of size $L_x \times L_y \times L_z$ ($L_z = 4.23$ nm for (n,0) nanotubes, and $L_z = 4.3959$ nm for (n,n) nanotubes) with periodic boundary conditions and minimum image convention for computing molecular interactions in x, y, and z directions, as presented in Figure 1.[68] We kept atomistic carbon nanotubes rigid in our computer experiments. Overall, we computed 28 CO_2 adsorption isotherms at 298 K and pressures from 1×10^{-6} to 5.7 MPa. More precisely, we studied CO_2 adsorption in nine bundles of SWNTs composed of the following armchair nanotubes: (8,8), (10,10), (12,12), (16,16), (20,20), (24,24), (28,28), (32,32), and (36,36). For comparison, we investigated CO_2 adsorption at 298 K in 19 SWNTs built up from the following chiral nanotubes: (12,0), (18,0), (24,0), (30,0), (36,0), (42,0), (48,0), (54,0), (60,0), (72,0), (84,0), (96,0), (108,0), (120,0), (132,0), (144,0), (156,0), (168,0), and (180,0). All simulated adsorption isotherms of CO_2 consisted of 94 points and covered the range of nanotube pore diameters, $D_{CYL} \in [0.93,14]$ nm.

As previously, the diameter of carbon nanotubes forming the bundle assembly was selected based on the assumed carbon−carbon bond length of $d_{CC} = 0.141$ nm, and given by the equation[68]

$$D_{CYL} = \frac{d_{CC}\sqrt{3(n^2 + n\cdot m + m^2)}}{\pi} \quad (5)$$

where (n,m) denotes the chiral vector of carbon nanotubes forming a bundle assembly. All studied bundles of SWNTs were constructed by using Nanotube Modeler software.[74] The grand canonical ensemble simulations utilized 5×10^7 configurations; the first 2.5×10^7 configurations were discarded to guarantee equilibration.

2.3. Gravimetric and Volumetric Storage of Carbon Dioxide. Packing of linear CO_2 molecules into studied carbon nanomaterials is essential for microscopic understanding of storage efficiency. The optimal porous materials for storage should maximize both gravimetric and volumetric uptake of CO_2 at given operating conditions. Thus, any objective statement about the storage efficiency of nanoporous material taken only from volumetric or gravimetric experimental measurements or computational experiments is incomplete. Some nanoporous materials can enhance the gravimetric density of adsorbed fluid significantly. However, at the same time, the pore density of trapped fluid can be quite low (for details, see Kowalczyk et al.[66,75]).

To determine the volumetric uptake of adsorbed CO_2 in studied carbon nanomaterials, we computed the absolute value of adsorption from the following formula[76,77]

$$\rho_{abs} = \frac{\langle N \rangle}{V\cdot N_{AV}} \quad (6)$$

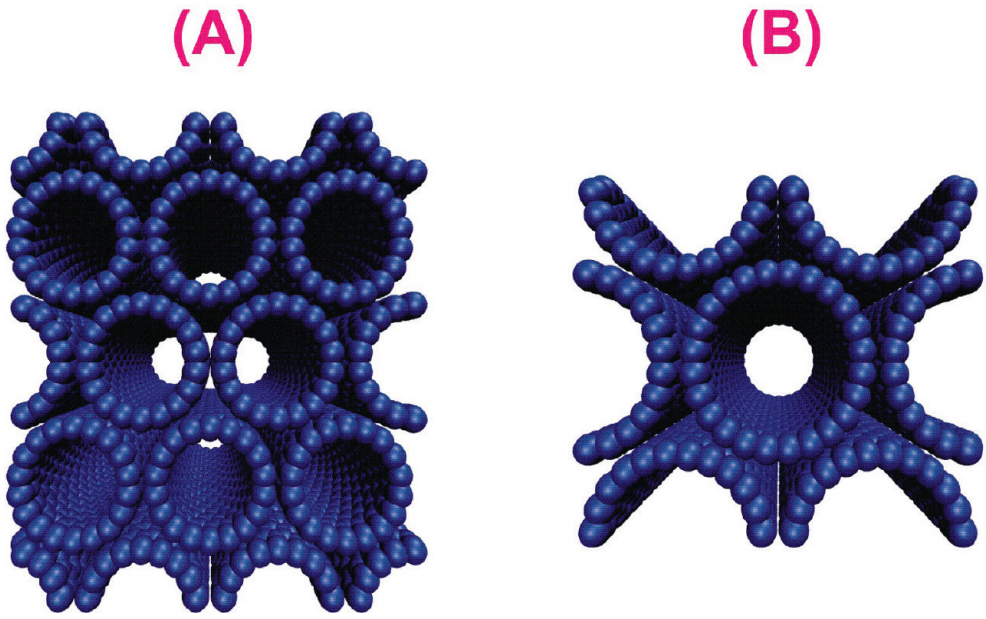

Figure 1. Carbon nanomaterials composed of single-walled nanotube bundles. We used the geometry of the carbon nanomaterial displayed in panel (A) for modeling of CO_2 adsorption at 298 K in smaller nanotubes [including (12,0), (18,0), (8,8), and (10,10)]. For remanning carbon nanomaterials built up from wider nanotubes, we adopted the geometry presented in panel (B). As an example, we show carbon nanomaterial composed of (18,0) (panel A) and (24,0) (panel B) SWNTs.

where $\langle N \rangle$ is the ensemble average of the number of CO_2 in the simulation box of volume $V = L_x L_y L_z$ and N_{AV} denotes Avogadro's number.

The gravimetric uptake of CO_2 adsorbed in studied carbon nanomaterials is simply given by[76,77]

$$\Gamma = \frac{\langle N \rangle}{N_C \cdot M_C} \tag{7}$$

where N_C denotes number of carbon atoms in the simulation box and M_C is the molecular mass carbon. The enthalpy of CO_2 adsorption was calculated from the theory of fluctuations.[76,77]

3. Results and Discussion

The accuracy of computer simulations strongly depends on the applied force field. In the current paper, we study the thermodynamic properties of CO_2 adsorbed in various nanoporous, microporous, and mesoporous carbon nanomaterials at 298 K. Note that this temperature is very close to 304 K (i.e., CO_2 critical temperature). Thus, the validation of the applied force field against known experimental data near the CO_2 bulk critical temperature is necessary. As one can see from Figure 2, the force field proposed by Nguyen[78] reproduces experimental data reasonably well.[79] The experimental CO_2 equation of state is quantitatively reproduced at 298, 320, and 340 K. Next, as shown in Figure 2, almost quantitative prediction of isothermal expansivity is achieved for CO_2, either in the vapor, liquid, or near-critical phase. Below the saturation pressure at 298 K, CO_2 is in the vapor state, and its thermal expansivity increases with increasing pressure. For very low pressures, the isothermal expansion would be expected to be $1/T = 1/(298\ \text{K}) = 0.00336\ \text{K}^{-1}$ due to the perfect gas law, which is correct at low pressures.[76,77] Our simulation results predicted the isothermal expansion of CO_2 of $0.00334\ \text{K}^{-1}$ at 0.1 MPa and 298 K, in agreement with the ideal gas law. Above the saturation pressure, isothermal expansivity is reduced since CO_2 is in a liquid state, and the density slowly increases with the increasing pressure,

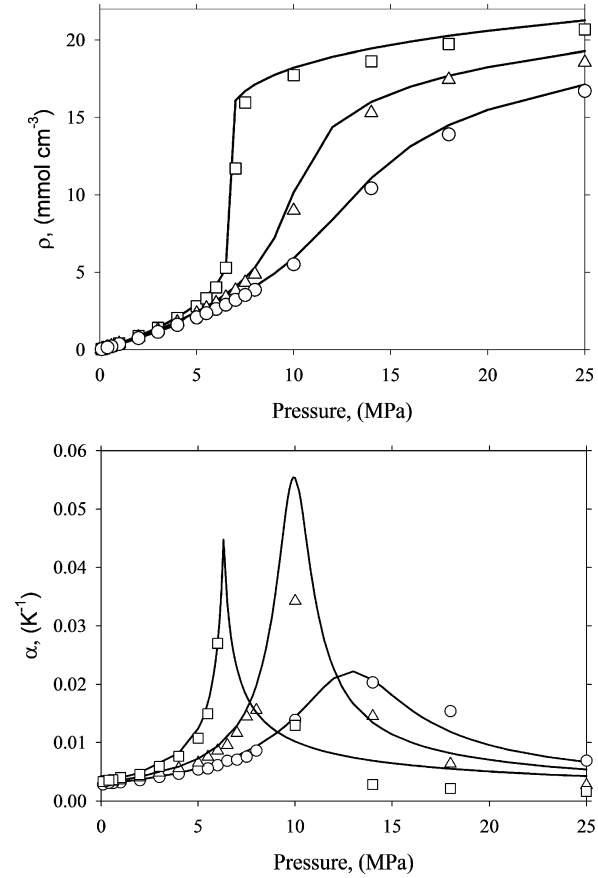

Figure 2. Reproduction of the experimental equation of state (upper panel) and isothermal expansivity[79] (bottom panel) for CO_2 at 298 (open squares), 320 (open triangles), and 340 K (open circles) by a three-center rigid model of CO_2 with a set of parameters taken from Nguyen[78] (see Table 1).

as displayed in Figure 2. Above the critical temperature of the CO_2 simulation, results clearly indicate that the isothermal expansivity is reduced (i.e., the single peak broadens and moves

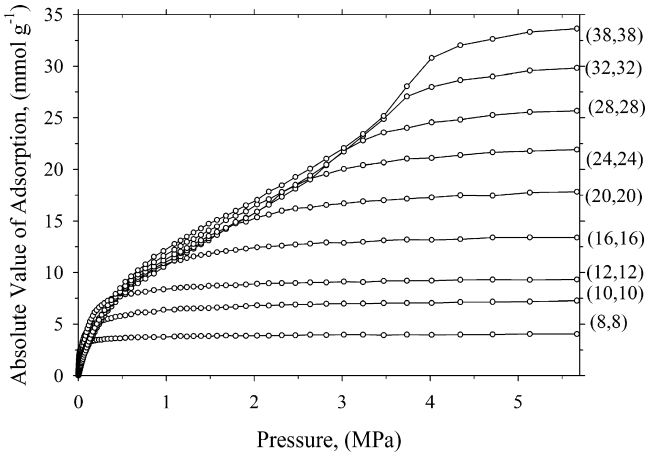

Figure 3. Pressure variation of the absolute value of CO_2 adsorption in selected carbon nanomaterials composed of armchair nanotubes at 298 K (the chiral vector is displayed on the plot).

to the higher values of pressures), in good agreement with the experimental data. Concluding, we are confident that the applied force field correctly reproduces thermodynamic properties of CO_2 near its critical temperature.

Selected CO_2 adsorption isotherms at 298 K on studied carbon nanomaterials composed of armchair SWNTs are displayed in Figure 3. First, we find that both volumetric and gravimetric uptake of CO_2 at 298 K strongly depend on the size of the nanotubes but not on their chiral vectors (i.e., detailed arrangement of carbon atoms on the nanotube surface). At the high temperature studied, adsorbed CO_2 molecules do not see details of the carbon surface because of their high kinetic energy. As expected, for all studied sizes of carbon nanotubes, the simulated adsorption isotherms exhibit type I behavior according to IUPAC classification.[60] However, widening of carbon nanotubes results in gradual CO_2 adsorption uptake, suggesting the presence of wider microporosity and small mesoporosity. This transformation of adsorption isotherms stems from a "cooperative pore filling"[80−82] mechanism of CO_2 adsorption in wider carbon nanotubes and interstitial channels. More precisely, for carbon nanomaterials built up from small nanotubes, the adsorption is governed by the "micropore filling" mechanism.[83−85] Gaseous CO_2 fills the internal and interstitial channels at low pressures because the strong solid−fluid potential alters vapor−liquid transformation of the adsorbed fluid. Interestingly, CO_2 molecules adsorbed in interstitial channels between carbon nanotubes form quasi-one-dimensional dense structures stabilized by the strong solid−fluid potential (see Figure 4 and the movie in the Supporting Information). At higher pressures, adsorbed CO_2 molecules are only slightly compressed due to geometric restrictions and the contribution of repulsive forces. In contrast, in carbon nanomaterials composed of wider nanotubes, the adsorption mechanism corresponds to the filling process by the CO_2 molecules in the mono- and multilayer-coated micropore walls (see Figure 5 and the movie in the Supporting Information). Similarly, in wider interstitial channels, the formation of discrete CO_2 layers occurs at low pressures. As the external pressure increases, the interstitial channels are filled by CO_2 molecules.

The highest enthalpy of CO_2 adsorption at 298 K and zero coverage of ~31 kJ mol^{-1} corresponds to bundles composed of (12,12) and (16,16) carbon nanotubes (equivalent pore diameters of 1.62 and 2.16 nm, respectively). As expected,

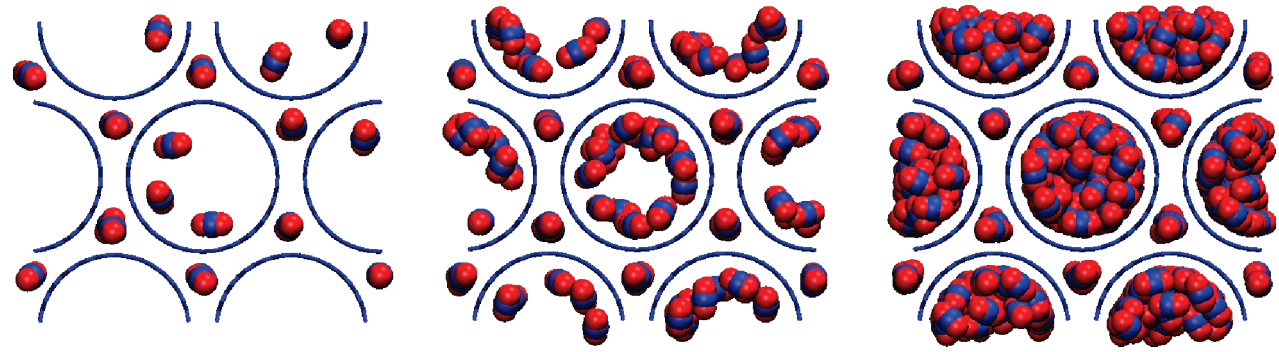

Figure 4. Snapshots of CO_2 adsorbed in a carbon nanomaterial composed of (24,0) single-walled nanotubes (equivalent pore diameter of 1.87 nm) at 298 K. The operating external pressures are 0.004 (left panel), 0.03 (middle panel), and 3.47 MPa (right panel). Note that CO_2 adsorbed in interstitial channels between cylindrical carbon pores form quasi-one-dimensional dense structures stabilized by a strong solid−fluid potential.

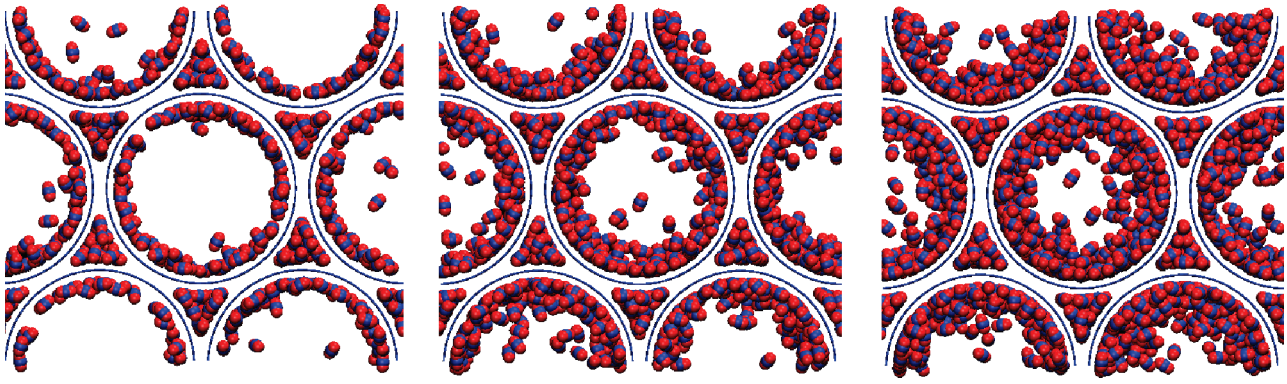

Figure 5. Snapshots of CO_2 adsorbed in a carbon nanomaterial composed of (60,0) single-walled nanotubes (equivalent pore diameter of 4.66 nm) at 298 K. The operating external pressures are 0.15 (left panel), 0.53 (middle panel), and 1.32 MPa (right panel). Note the multilayer formation and growth of adsorbed CO_2 layers in internal cylindrical carbon pores.

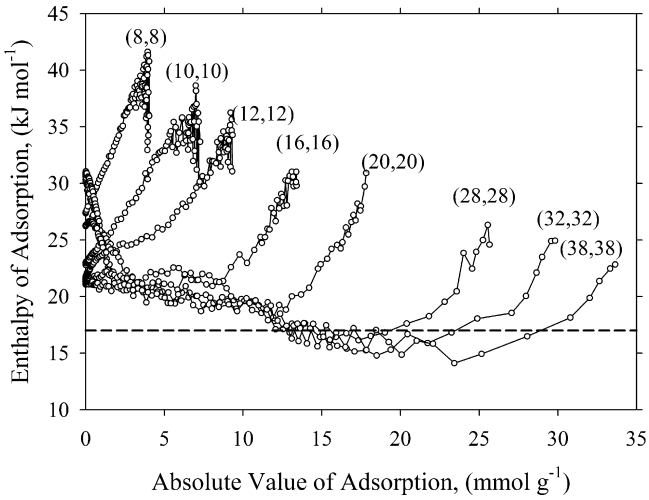

Figure 6. Variation of the enthalpy of CO_2 adsorption with the absolute value of adsorption, for selected carbon nanomaterials at 298 K (the chiral vector is displayed on the plot). For comparison, the enthalpy of CO_2 liquefaction (17 kJ mol^{-1})[89] is shown by the dashed line. Note that the enthalpy of CO_2 for monolayer adsorption on the basal plane of graphite of 22.7−25.3 kJ mol^{-1} is reproduced for carbon nanomaterials composed of wider nanotubes at zero coverage.[86]

widening of carbon nanotubes reduces the enthalpy of CO_2 adsorption at zero coverage because of the rapid decrease in the solid−fluid interaction potential, as shown in Figure 6. Reduction in nanotube sizes decreases the enthalpy of CO_2 adsorption at 298 K and zero converge as well. This is caused by the imperfect packing of adsorbed rod-shaped CO_2 molecules in restricted geometries as well as the contribution of repulsion forces in very small nanospaces. We want to point out that the enthalpy of CO_2 adsorption at 298 K and zero converge corresponding to bundle composed of (10,10) SWNTs of 23 kJ mol^{-1} coincides with experimentally reported values of 22.5−23 kJ mol^{-1}.[86] This is because the bundles of (10,10) and similar nanotubes are the most abundant ones.

Detailed inspection results of CO_2 local densities in selected carbon nanomaterials and operating conditions are displayed in Figures 7 and 8. We find that near ambient operating pressures, the adsorbed and compressed CO_2 form two and three dense concentric solid-like layers in carbon nanotubes of pore diameter ≈ 2 nm. As we showed above, this size of carbon nanotubes corresponds to the highest enthalpy of CO_2 adsorption at 298 K and zero coverage. That is why the carbon nanomaterials composed of nanotubes with the quoted pore diameter maximized volumetric storage of CO_2 at 298 K, as shown in Figure 9. One can conclude that these carbon nanomaterials are optimal for short-term reversible storage of CO_2 near ambient operating conditions. However, this is not the case because the maximum of volumetric CO_2 uptake does not correspond to maximum CO_2 uptake per mass of carbon nanomaterial. We studied this important issue in detail.

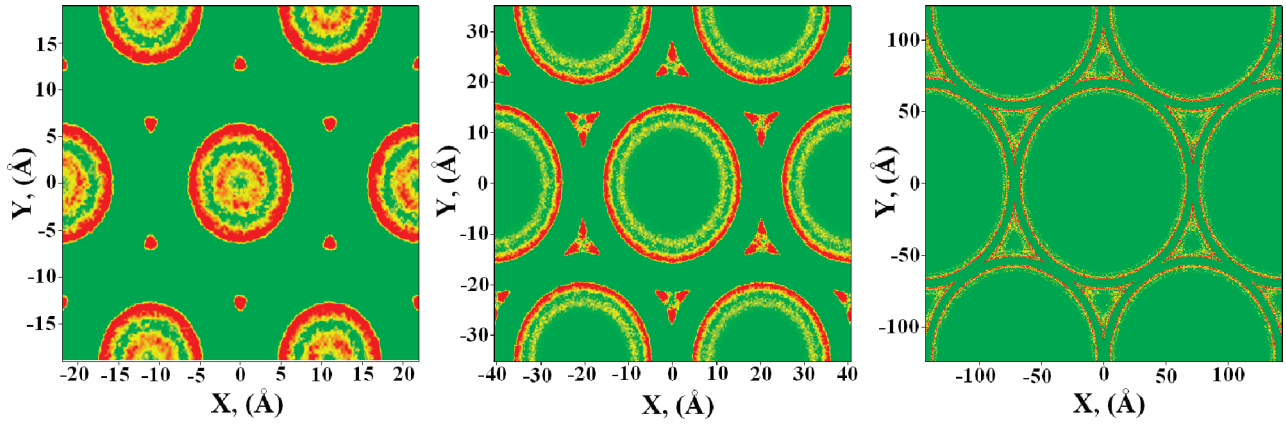

Figure 7. Local density profiles of CO_2 adsorbed in selected carbon nanomaterials built up from different nanotubes [from left to right, (24,0), (48,0), and (180,0)] at 1.48 MPa an 298 K. The middle panel corresponds to a bundle composed of (48,0) SWNTs (i.e., equivalent pore diameter of 3.7 nm) that maximizes both volumetric and gravimetric CO_2 storage at 1.48 MPa and 298 K.

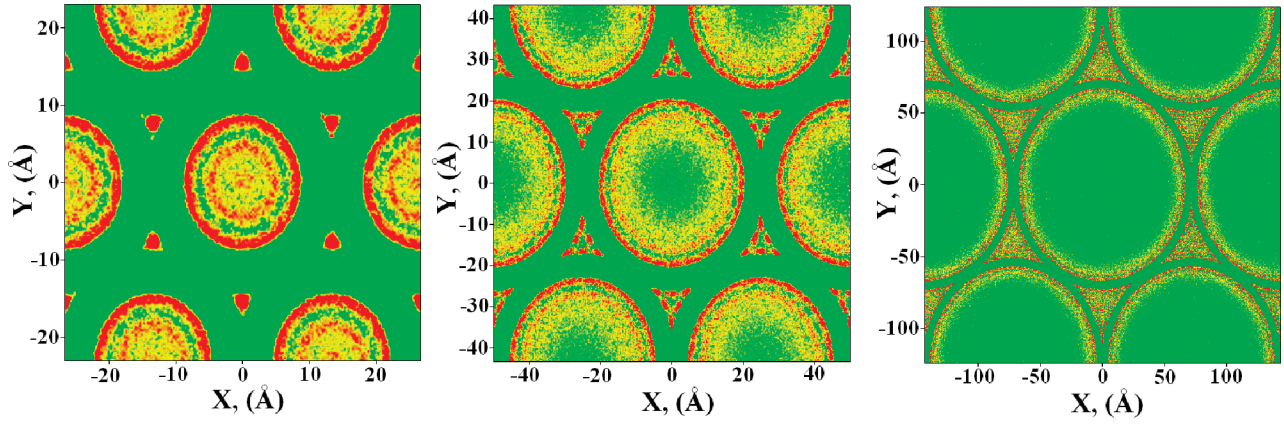

Figure 8. Local density profiles of CO_2 adsorbed in selected carbon nanomaterials built up from different nanotubes [from left to right, (30,0), (60,0), and (180,0)] at 3.47 MPa an 298 K. The middle panel corresponds to a bundle composed of (60,0) SWNTs (i.e., equivalent pore diameter of 4.7 nm) that maximizes both volumetric and gravimetric CO_2 storage at 3.47 MPa and 298 K.

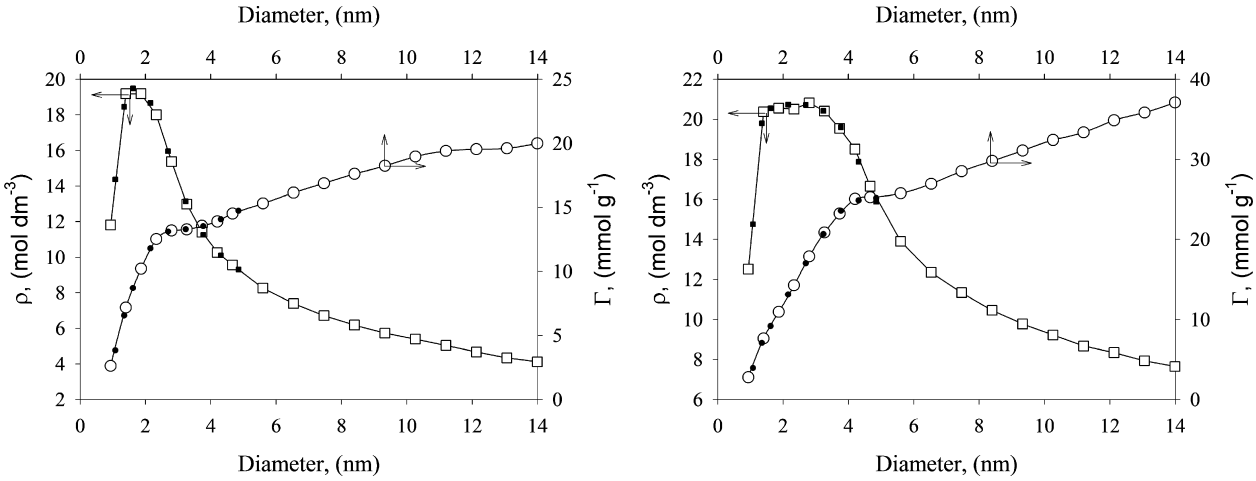

Figure 9. Gravimetric and volumetric CO_2 uptake at 298 K in studied carbon nanomaterials composed of armchair nanotubes (black circles) and chiral nanotubes (opens squares and circles). The external pressures are 1.5 (left panel) and 3.5 MPa (right panel). Note that the density of liquid CO_2 at 298 K is 17.6 mol dm^{-3}.

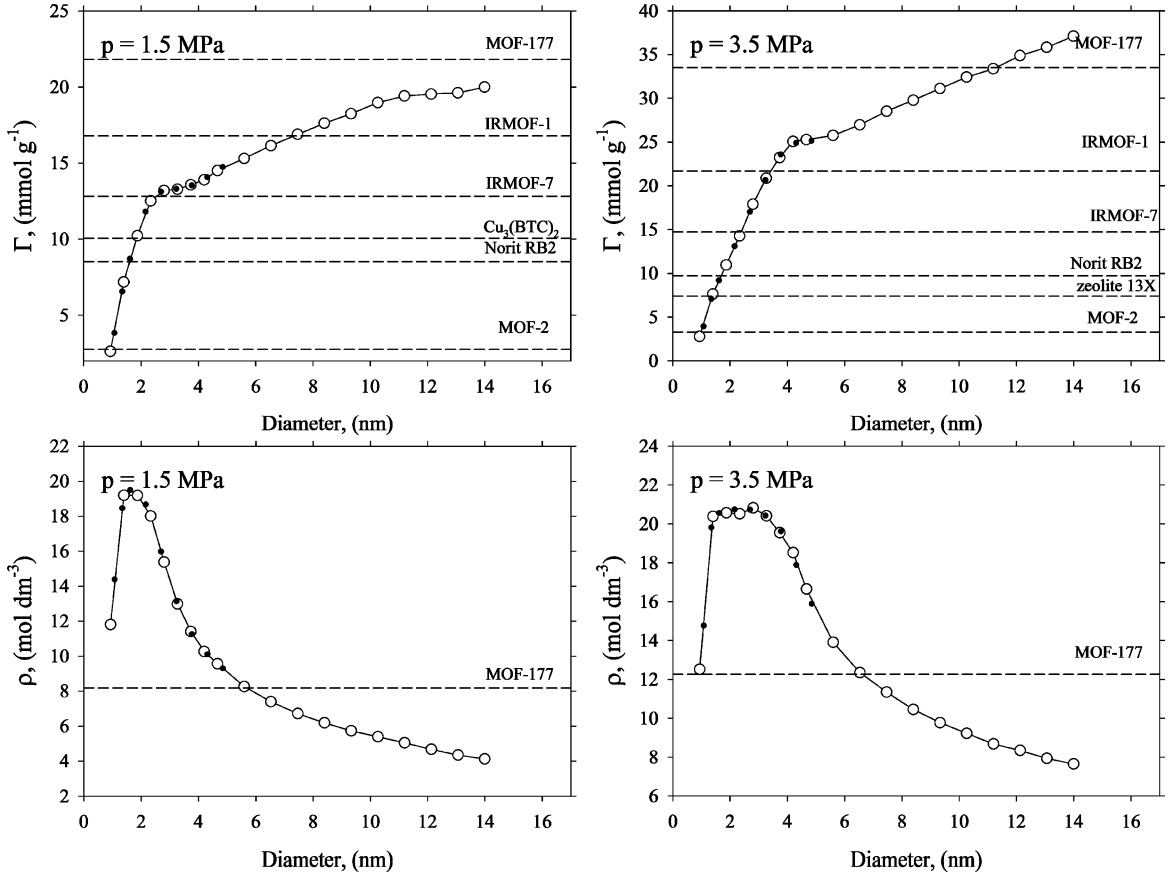

Figure 10. Comparison of gravimetric and volumetric CO_2 uptake at 298 K in studied carbon nanomaterials (black circles: armchair nanotubes; opens squares and circles: chiral nanotubes) and selected ordinary and novel nanoporous materials.[87] Note that the experimental density of CO_2 in MOF-177 at 1.5 and 3.5 MPa indicates that the adsorbed CO_2 is in a compressed gas state at 298 K.

Both gravimetric and volumetric storage of CO_2 at studied operating conditions strongly depend on the size of the carbon nanotubes (see Figure 9). The highest average density of adsorbed and compressed CO_2 exceeds 17.6 mol dm^{-3} (i.e., density of liquid CO_2 at 298 K). Further, both volumetric and gravimetric CO_2 uptake slightly depend on the selected operating pressure. More precisely, the highest volumetric storage of CO_2 at 1.5 MPa ($\sim$19−20 mol dm^{-3}) corresponds to nanotube diameters of $\sim$1.4−2.3 nm. For a higher operating pressure of 3.5 MPa, these densities of adsorbed CO_2 can be achieved in wider rage of nanotube sizes (i.e., nanotube diameter $\approx$ 1.4−3.7 nm). In contrast, the gravimetric storage of CO_2 is continuously increasing with the mass of carbon (i.e., the size of carbon nanotubes composing the bundle structure), as displayed in Figure 9. In carbon nanomaterials composed of wider nanotubes, CO_2 is only adsorbed in the interstitial channels between carbon nanotubes and slightly in the internal cylindrical pores (see the discrete concentric layers of adsorbed CO_2 shown in Figures 7 and 8). Almost all internal cylindrical carbon pores are filled by gaseous CO_2. Taking both volumetric and gravimetric CO_2 uptake, we concluded that the optimal size of carbon nanotubes for assumed operating pressures can be uniquely defined. At

1.5 MPa and 298 K, the most efficient nanotubes that maximize both gravimetric and volumetric uptake of CO_2 (13.6 mmol g^{-1} and 11.4 mol dm^{-3}) have diameters of 3.8 nm, as presented in Figure 9. This size corresponds to the (28,28) armchair nanotubes. For a higher operating pressure of 3.5 MPa, the optimal diameter of carbon nanotubes is slightly shifted up to 4.8 nm (25.3 mmol g^{-1} and 16.7 mol dm^{-3}). This size corresponds to the (36,36) armchair nanotubes. Concluding, the optimal carbon nanomaterials for short-term reversible storage of CO_2 at 298 K and near ambient operating pressures are composed of wider nanotubes. Further, the enthalpy of CO_2 adsorption cannot be used as a unique measure of storage efficiency because of the subtle balance between the binding energy and excluded volumes.

Finally, we compare our simulation results with experimental CO_2 data reported in the literature. Unfortunately, in almost all experimental reports, the adsorption data are incomplete. The experimentalists usually report gravimetric uptake of CO_2 without any additional information about the average density of adsorbed fluid. As one can see from Figure 9, very high gravimetric uptake of CO_2 can be easily achieved in carbon nanomaterials composed of large-diameter carbon nanotubes. At the same time, the volumetric CO_2 is drastically reduced due to a rapid decrease of the solid−fluid dispersion energy. To critically discuss the applicability of different materials for short-term reversible storage of CO_2, the complete volumetric and gravimetric adsorption data are necessary. Taking into account both gravimetric and volumetric CO_2 uptake, we find that carbon nanomaterials composed of optimized SWNTs are superior storage vessels in comparison to ordinary porous materials, such as Norit RB2 and zeolite 13X[87] (see Figures 9 and 10). The gravimetric uptake of activated carbons is inevitably lowered by their structural heterogeneities, whereas the size of microporous zeolite channels is too small to accommodate the high mass of adsorbed CO_2 molecules. The adsorption properties of novel MOFs are more interesting. The most promising MOF-177 adsorbs a large mass of CO_2 per mass of the nonmaterial,[87] as shown in Figure 10. However, the reported volumetric uptake of CO_2 at 298 K and 1.5 MPa of 8.2 mol dm^{-3} (that at 3.5 MPa of 12.3 mol dm^{-3}) is lower in comparison to that of carbon nanomaterials composed of optimized nanotubes. The experimental densities of CO_2 in MOF-177 at 298 K and studied storage pressures indicate that adsorbed CO_2 molecules are not in the liquid state. Indeed, the gradual shape of the CO_2 adsorption isotherm in MOF-177 is similar to that corresponding to studied carbon nanomaterials composed of wider nanotubes (compare Figure 2 in ref 87 and Figure 3). The remaining important technological issue is the instability of MOF-177 in real operating conditions. It has been shown that MOF-177 easily decomposes, forming nonporous amorphous material due to small amounts of water vapor in the adsorbed mixture.[88] Carbonaceous nanomaterials are stable in both dry and moist atmospheres. Concluding, we argue that carbonaceous nanomaterials composed of the optimized single-walled nanotubes are attractive candidates for innovation in clean technologies. The performance of studied carbon nanomaterials for separation of CO_2 from the industrial exhaust gases of combustion will be the subject of our future works.

4. Conclusions

Light nanomaterials composed of optimized SWNTs have high gravimetric and volumetric capacity for storage of CO_2 at 298 K and near ambient operating pressures. Both gravimetric and volumetric storage of CO_2 strongly depend on the pore size in nanotubes. We show that for any operating storage pressure, a unique optimal size of carbon nanotubes is well-defined. Therefore, at 1.5 MPa, the most efficient nanotubes that maximize both gravimetric and volumetric uptake of CO_2 (13.6 mmol g^{-1} and 11.4 mol dm^{-3}) have diameters of 3.8 nm. This size corresponds to the (28,28) armchair nanotubes. At 3.5 MPa, the optimal diameter of carbon nanotubes is slightly shifted up to 4.8 nm (25.3 mmol g^{-1} and 16.7 mol dm^{-3}). This size corresponds to the (36,36) armchair nanotubes. We clearly demonstrate that to make an objective statement about the efficiency of CO_2 storage in any nanoporous material, the complete volumetric and gravimetric adsorption data are necessary. We show that very high gravimetric CO_2 uptake can be achieved in carbon nanomaterials composed of large-diameter nanotubes. However, for the same operating conditions, the density of adsorbed CO_2 is very low in comparison to its liquid one. Taking this insight into account, we critically discuss the exceptionally high capacity of MOFs reported recently. We show that MOF-177, known as the most efficient porous material for storage of CO_2 at room temperature, is characterized by very high gravimetric uptake of CO_2 (i.e., 21.8 mmol g^{-1} at 1.5 MPa and 33.5 mmol g^{-1} at 3.5 MPa). However, the volumetric density of CO_2 in MOF-177 at 298 K (i.e., 8.17 mol dm^{-3} at 1.5 MPa and 12.26 mol dm^{-3} at 3.5 MPa) is lower in comparison to that of the studied carbon nanomaterials composed of optimized nanotubes. CO_2 molecules adsorbed in MOF-177 are not in the liquid but compressed gas state.

Acknowledgment. P.K. acknowledges the use of the computer clusters VPAC (Victorian Partnership for Advanced Computing, Melbourne, Australia). P.K. acknowledges the Curtin University of Technology for a senior research fellowship. P.G. and A.P.T. acknowledge the use of the computer cluster at the Poznan Supercomputing and Networking Centre as well as the Information and Communication Technology Centre of the Nicolaus Copernicus University (Torun, Poland). S.F. gratefully acknowledges financial support from the Foundation for Polish Science.

Supporting Information Available: Snapshots of CO_2 adsorbed in selected carbon nanomaterials composed of SWNTs. Additional simulation results for selected values of the solid−fluid LJ well depth (Figure 1S and 2S). It should be noted that some figures (showing the snapshots of the animations, i.e. Figure 1, 4, and 5) and all movies in the Supporting Information were created using the VMD program.[90,91] This material is available free of charge via the Internet at http://pubs.acs.org.

References and Notes

(1) Takahashi, T. *Science* **2004**, *305*, 352.
(2) Sabine, Ch. L.; Feely, R. A.; Gruber, N.; Key, R. M.; Lee, K.; Bullister, J. L.; Wanninkhof, R.; Wong, C. S.; Wallace, D. W. R.; Tilbrook, B.; Millero, F. J.; Peng, T. H.; Kozyr, A.; Ono, T.; Rios, A. F. *Science* **2004**, *305*, 367.
(3) Brewer, P. G. *Proc. Natl. Acad. Sci. U.S.A.* **2009**, *106*, 12213.
(4) Riebesell, U.; Körtzinger, A.; Oschlies, A. *Proc. Natl. Acad. Sci. U.S.A.* **2009**, *106*, 20602.
(5) Manzello, D. P.; Kleypas, J. A.; Budd, D. A.; Eakin, C. M.; Glynn, P. W.; Langdon, C. *Proc. Natl. Acad. Sci. U.S.A.* **2008**, *105*, 10450.
(6) Riebesell, U.; Zondervan, I.; Rost, B.; Tortell, P. D.; Zeebe, R. E.; Morel, F. M. M. *Nature* **2000**, *407*, 364.
(7) Feely, R. A.; Sabine, Ch. L.; Lee, K.; Berelson, W.; Kleypas, J.; Fabry, V. J.; Millero, F. J. *Science* **2004**, *305*, 362.
(8) Ries, J. B.; Cohen, A. L.; McCorkle, D. C. *Geology* **2009**, *37*, 1131.
(9) Petit, J. R.; Jouzel, J.; Raynaud, D.; Barkov, N. I.; Barnola, J. M.; Basile, I.; Bender, M.; Chappellaz, J.; Davis, M.; Delaygue, G.; Delmotte, M.; Kotlyakov, M. V.; Legrand, M.; Lipenkov, V. Y.; Lorius, C.; PÉpin, L.; Ritz, C.; Saltzman, E.; Stievenard, M. *Nature* **1999**, *399*, 429.
(10) Sigman, D. M.; Boyle, E. A. *Nature* **2000**, *407*, 859.

(11) Lackner, K. S. *Science* **2003**, *300*, 1677.
(12) Witze, A. *Nature* **2008**, *456*, 290.
(13) Kowalczyk, P.; Furmaniak, S.; Gauden, P. A.; Terzyk, A. P. *J. Phys. Chem. C* **2010**, *114*, 5126.
(14) Yazaydin, A. O.; Snurr, R. Q.; Park, T. H.; Koh, K.; Liu, J.; LeVan, M. D.; Benin, A. I.; Jakubczak, P.; Lanuza, M.; Galloway, D. B.; Low, J. J.; Willis, R. R. *J. Am. Chem. Soc.* **2009**, *131*, 18198.
(15) Yazaydin, A. O.; Benin, A. I.; Faheem, S. A.; Jakubczak, P.; Low, J. J.; Willis, R. R.; Snurr, R. Q. *Chem. Mater.* **2009**, *21*, 1425.
(16) Babarao, R.; Jiang, J.; Sandler, S. I. *Langmuir* **2009**, *25*, 5239.
(17) Keskin, S.; Liu, J.; Rankin, R. B.; Johnson, J. K.; Sholl, D. S. *Ind. Eng. Chem. Res.* **2009**, *48*, 2355.
(18) Haldoupis, E.; Nair, S.; Sholl, D. S. *J. Am. Chem. Soc.* **2010**, *132*, 7528.
(19) Jee., S. E.; Sholl, D. S. *J. Am. Chem. Soc.* **2009**, *131*, 7896.
(20) Sirevåg, R.; Ormerod, J. G. *Science* **1970**, *169*, 186.
(21) Karagouni, A. D.; Kelly, D. P. *FEMS Microbiol. Lett.* **1989**, *58*, 179.
(22) Paddock, R. L.; Nguyen, S. T. *J. Am. Chem. Soc.* **2001**, *123*, 11498.
(23) Zevenhovena, R.; Eloneva, S.; Teir, S. *Catal. Today* **2006**, *115*, 73.
(24) Brewer, P. G.; Friederich, G.; Peltzer, E. T.; Orr, F. M., Jr. *Science* **1999**, *284*, 943.
(25) Rau, G. H.; Caldeira, K. *Science* **2002**, *276*, 275.
(26) Haugan, P. M.; Drange, H. *Nature* **1992**, *357*, 318.
(27) Auerbach, S. M.; Carrado, K. A.; Dutta, P. K. *Handbook of Zeolite Science and Technology*; Marcel Dekker, Inc.: New York, 2003.
(28) Yang, R. T. *Gas Separation by Adsorption Processes*; Imperial Colleague Press: London, 1997.
(29) Do, D. D. *Adsorption Analysis: Equilibria and Kinetics*; ICP: London, 1998.
(30) Marsh, H.; Rodriguez-Reinoso, F. *Activated Carbon*; Elsevier Ltd.: Oxford, U.K., 2006.
(31) Kowalczyk, P.; Terzyk, A. P.; Gauden, P. A.; Leboda, R.; Szmechtig-Gauden, E.; Rychlicki, G.; Ryu, Z.; Rong, H. *Carbon* **2003**, *41*, 1113.
(32) Kowalczyk, P.; Tanaka, H.; Holyst, R.; Kaneko, K.; Ohmori, T.; Miyamoto, J. *J. Phys. Chem. B* **2005**, *109*, 17174.
(33) Bansal, R. Ch., Goyal, M. *Activated Carbon Adsorption*; CRC Press: Boca Raton, FL, 2005.
(34) Kärger, J.; Ruthven, D. M. *Diffusion in Zeolites and Other Microporous Solids*; John Wiley & Sons: New York, 1992.
(35) Kondo, A.; Noguchi, H.; Ohnishi, S.; Kajiro, H.; Tohdoh, A.; Hattori, Y.; Xu, W.-Ch.; Tanaka, H.; Kanoh, H.; Kaneko, K. *Nano Lett.* **2006**, *6*, 2581.
(36) Britt, D.; Furukawa, H.; Wang, B.; Glover, T. G.; Yaghi, O. M. *Proc. Natl. Acad. Sci. U.S.A.* **2009**, *106*, 20637.
(37) Banerjee, R.; Phan, A.; Wang, B.; Knobler, C.; Furukawa, H.; O'Keeffe, M.; Yaghi, O. M. *Science* **2008**, *319*, 939.
(38) Furukawa, H.; Yaghi, O. M. *J. Am. Chem. Soc.* **2009**, *25*, 886.
(39) Kitagawa, S.; Kitaura, R.; Noro, S. I. *Angew. Chem., Int. Ed.* **2004**, *43*, 2334.
(40) Matsuda, R.; Kitaura, R.; Kitagawa, S.; Kubota, Y.; Kobayashi, T. C.; Horike, S.; Takata, M. *J. Am. Chem. Soc.* **2004**, *125*, 14063.
(41) Kondo, A.; Noguchi, H.; Carlucci, L.; Proserpio, D. M.; Ciani, G.; Kajiro, H.; Ohba, T.; Kanoh, H.; Kaneko, K. *J. Am. Chem. Soc.* **2007**, *127*, 12362.
(42) Yaghi, O. M. *Nat. Mater.* **2007**, *6*, 92.
(43) Iijima, S. *Nature* **1991**, *354*, 56.
(44) Iijima, S.; Yudasaka, M.; Yamada, R.; Bandow, S.; Suenaga, K.; Kokai, F. *Chem. Phys. Lett.* **1999**, *309*, 165.
(45) Gogotsi, Y.; Dash, R. K.; Yushin, G.; Yildrim, T.; Laudisio, G.; Fischer, J. E. *J. Am. Chem. Soc.* **2005**, *127*, 16006.
(46) Kowalczyk, P.; Jaroniec, M.; Solarz, L.; Terzyk, A. P.; Gauden, P. A. *Adsorpt. Sci. Technol.* **2006**, *24*, 411.
(47) Endo, M.; Muramatsu, H.; Hayashi, T.; Kim, Y. A.; Terrones, M.; Dresselhaus, M. S. *Nature* **2005**, *433*, 476.
(48) Tao, Y.; Muramatsu, H.; Endo, M.; Kaneko, K. *J. Am. Chem. Soc.* **2010**, *132*, 1214.
(49) Kowalczyk, P.; Solarz, L.; Do, D. D.; Samborski, A.; MacElroy, J. M. *Langmuir* **2006**, *22*, 9035.
(50) Kowalczyk, P.; Gauden, P. A.; Terzyk, A. P. *J. Phys. Chem. B* **2008**, *112*, 8275.
(51) Ryoo, R.; Joo, S. H.; Jun, S. *J. Phys. Chem. B* **1999**, *103*, 7743.
(52) Ryoo, R.; Joo, S. H.; Kruk, M.; Jaroniec, M. *Adv. Mater.* **2001**, *13*, 677.
(53) Kyotani, T.; Nagai, T.; Inoue, S.; Tomita, A. *Chem. Mater.* **1997**, *9*, 609.
(54) Endo, M.; Kim, Y. A.; Ezaka, M.; Osada, K.; Yanagisawa, T.; Hayashi, T.; Terrones, M.; Dresselhaus, M. S. *Nano Lett.* **2003**, *3*, 723.
(55) Terrones, M. *Nature* **2009**, *458*, 845.
(56) Terrones, H.; Terrones, M. *Carbon* **1998**, *36*, 725.
(57) Terzyk, A. P., Gauden, P. A., Kowalczyk, P., Eds. *Carbon Materials — Theory and Practice*; Research Signpost: Kerala, India, 2008.
(58) Dunne, L. J., Manos, G., Eds. *Adsorption and Phase Behaviour in Nanochannels and Nanotubes*; Springer: Dordrecht, The Netherlands, 2010.
(59) Cinke, M.; Li, J.; Bauschlicher Jr., Ch. W.; Ricca, A.; Meyyappan, M. *Chem. Phys. Lett.* **2003**, *376*, 761.
(60) Sing, K. S. W.; Everett, D. H.; Haul, R. A. W.; Moscou, L.; Pierotti, R. A.; Rouquérol, J.; Siemieniewska, T. *Pure Appl. Chem.* **1985**, *57*, 603.
(61) Brunauer, S.; Emmett, P. H.; Teller, E. *J. Am. Chem. Soc.* **1938**, *60*, 309.
(62) Shen, Y.; Bai, J. *Chem. Commun.* **2010**, *46*, 1308.
(63) Hsu, S.-Ch.; Lu, Ch.; Su, F.; Zeng, W.; Chen, W. *Chem. Eng. Sci.* **2010**, *65*, 1354.
(64) Huang, L.; Zhang, L.; Shao, Q.; Lu, L.; Lu, X.; Jiang, S.; Shen, W. *J. Phys. Chem. C* **2007**, *111*, 11912.
(65) Shi, W.; Johnson, J. K. *Phys. Rev. Lett.* **2003**, *91*, 015504.
(66) Kowalczyk, P.; Holyst, R. *Environ. Sci. Technol.* **2008**, *42*, 2931.
(67) Kowalczyk, P.; Brualla, L.; Żywociński, A.; Bhatia, S. K. *J. Phys. Chem. C* **2007**, *111*, 5250.
(68) Furmaniak, S.; Terzyk, A. P.; Gauden, P. A.; Wesołowski, R. P.; Kowalczyk, P. *Phys. Chem. Chem. Phys.* **2009**, *11*, 4982.
(69) Chen, L.; Johnson, J. K. *Phys. Rev. Lett.* **2005**, *94*, 125701.
(70) Terzyk, A. P.; Furmaniak, S.; Gauden, P. A.; Kowalczyk, P. *Adsorpt. Sci. Technol.* **2009**, *27*, 281.
(71) Allen, M. P.; Tildesley, D. J. *Computer Simulation of Liquids*; Clarendon: Oxford, U.K., 1987.
(72) Frenkel, D.; Smit, B. *Understanding Molecular Simulation From Algorithms To Applications*; Academic Press: London, 1996.
(73) Gray, C. G.; Gubbins, K. E. *Theory of Molecular Fluids*; Clarendon Press: Oxford, U.K., 1984; Vol. 1.
(74) Nanotube Modeler. http://www.jcrystal.com/products/wincnt/.
(75) Kowalczyk, P.; Holyst, R.; Terrones, M.; Terrones, H. *Phys. Chem. Chem. Phys.* **2007**, *9*, 1786.
(76) Nicholson, D.; Parsonage, N. G. *Computer Simulation and the Statistical Mechanics of Adsorption*; Academic Press: London, 1982.
(77) Ungerer, P.; Travitian, B.; Boutin, A. *Application of Molecular Simulation in the Oil and Gas Industry*; Editions Technip: Paris, 2005.
(78) Nguyen, T. X. Characterization of Nanoporous Carbons; Ph.D. Thesis, The University of Queensland, Brisbane, Australia, 2006.
(79) Vagraftik, N. B. *The Handbook of Thermodynamic Properties of Gases and Liquids*; G.I.F.M.L.: Moscow, 1963; in Russian.
(80) Setoyama, N.; Kaneko, K.; Rodriguez-Reinoso, F. *J. Phys. Chem.* **1996**, *100*, 10331.
(81) Kakei, K.; Ozeki, S.; Suzuki, T.; Kaneko, K. *J. Chem. Soc., Faraday Trans.* **1990**, *86*, 371.
(82) Setoyama, N.; Suzuki, T.; Kaneko, K. *Carbon* **1998**, *36*, 1459.
(83) Dubinin, M. M. In *Progress in Membrane and Surface Science*; Cadenhead, D. A., Ed.; Academic Press: New York, 1975; Vol. 9, p 1.
(84) Kowalczyk, P.; Terzyk, A. P.; Gauden, P. A. *Langmuir* **2002**, *18*, 5406.
(85) Rudzinski, W.; Everett, D. H. *Adsorption of Gases on Heterogeneous Surfaces*; Academic Press: New York, 1992.
(86) Bienfait, M.; Zeppenfeld, P.; Dupont-Pavlovsky, N.; Muris, M.; Johnson, M. R.; Wilson, T.; DePies, M.; Vilches, O. E. *Phys. Rev. B* **2004**, *70*, 035410.
(87) Millward, A. R.; Yaghi, O. M. *J. Am. Chem. Soc.* **2005**, *127*, 17998.
(88) Li, Y.; Yang, R. T. *Langmuir* **2007**, *23*, 12937.
(89) Demessence, A.; D'Alessandro, D. M.; Lin Foo, M.; Long, J. R. *J. Am. Chem. Soc.* **2009**, *131*, 8784.
(90) Humphrey, W.; Dalke, A.; Schulten, K. *J. Mol. Graphics* **1996**, *14*, 33.
(91) Visual Molecular Dynamics. http://www.ks.uiuc.edu/Research/vmd/.

JP106547J